

# Self-locked broadband Raman-electro-optic microcomb

Shuai Wan<sup>1,2,4,\*</sup>, Pi-Yu Wang<sup>1,2,4,\*</sup>, Ming Li<sup>1,2,4,\*</sup>, Rui Ma<sup>3</sup>, Rui Niu<sup>1,2,4</sup>,

Fang-Wen Sun<sup>1,2,4</sup>, Fang Bo<sup>3,†</sup>, Guang-Can Guo<sup>1,2,4</sup>, and Chun-Hua Dong<sup>1,2,4,‡</sup>

<sup>1</sup>*CAS Key Laboratory of Quantum Information, University of Science and Technology of China, Hefei, Anhui 230026, People's Republic of China*

<sup>2</sup>*CAS Center For Excellence in Quantum Information and Quantum Physics, University of Science and Technology of China, Hefei, Anhui 230088, People's Republic of China*

<sup>3</sup>*MOE Key Laboratory of Weak-Light Nonlinear Photonics, TEDA Applied Physics Institute and School of Physics,*

*Nankai University, Tianjin 300457, People's Republic of China and*

<sup>4</sup>*Hefei National Laboratory, University of Science and Technology of China, Hefei, Anhui 230088, People's Republic of China*

Optical frequency combs (OFCs), composed of equally spaced frequency tones, have spurred advancements in communications, spectroscopy, precision measurement and fundamental physics research. A prevalent method for generating OFCs involves the electro-optic (EO) effect, i.e., EO comb, renowned for its rapid tunability via precise microwave field control. Recent advances in integrated lithium niobate (LN) photonics have greatly enhanced the efficiency of EO effect, enabling the generation of broadband combs with reduced microwave power. However, parasitic nonlinear effects, such as Raman scattering and four-wave mixing, often emerge in high-quality nonlinear devices, impeding the expansion of comb bandwidth and the minimization of frequency noise. Here, we tame these nonlinear effects and present a novel type of OFC, i.e., the self-locked Raman-electro-optic (REO) microcomb by leveraging the collaboration of EO, Kerr and Raman scattering processes. The spectral width of the REO microcomb benefits from the Raman gain and Kerr effect, encompassing nearly 1400 comb lines spanning over 300 nm with a fine repetition rate of 26.03 GHz, much larger than the pure EO combs. Remarkably, the system can maintain a self-locked low-noise state in the presence of multiple nonlinearities without the need for external active feedback. Our approach points to a direction for improving the performance of microcombs and paves the way for exploring new nonlinear physics, such as new laser locking techniques, through the collaboration of inevitable multiple nonlinear effects in integrated photonics.

## I. INTRODUCTION

Integrated photonics has markedly revolutionized the generation and manipulation light on a microscale in recent years, heralding a new era in photonic technologies. One of the most transformative developments is the realization of optical frequency combs (OFCs) in on-chip nonlinear microresonators [1–6]. OFCs, consisting of evenly spaced discrete spectral lines, have emerged as essential tools in modern photonics, profoundly transforming fields like precision timing, spectroscopy, and high-speed communications [7–14]. Traditional OFCs, generated via mode-locked lasers, require bulky laboratory setups, limiting their practical applications outside laboratory environments [15–17]. Consequently, substantial efforts have been made to integrate OFCs into compact, chip-scale systems [18–21].

Currently, the primary approaches for generating on-chip OFCs are based on the Kerr effect, specifically dissipative Kerr solitons (DKSs), and the electro-optic (EO) effect, known as EO combs. While DKSs enable ultrafast, passive mode-locking and can facilitate envelope design and spectrum broadening through dispersion engineering, they require precise control and are sensitive to thermal fluctuations [4]. In contrast, EO combs, which have been implemented in lithium niobate resonators and

waveguides, are easier to generate and can be directly locked to microwave frequencies but exhibit limited spectral width and depend heavily on microwave power [22–25]. Additionally, the generation of OFCs is often accompanied by parasitic nonlinear effects, such as Raman scattering [26, 27] in material platforms like lithium niobate (LN) and lithium tantalate (LT). Raman scattering not only introduces additional frequency noise but also impedes the generation and extension of OFCs, necessitating special structural designs to suppress Raman excitations [28–31]. To fully leverage the advantages of both DKSs and EO combs while overcoming their inherent limitations and eliminating the impact of parasitic nonlinear effects, exploring the synergy of multiple nonlinear effects is a promising approach. However, the simultaneous occurrence and synergy of multiple nonlinear effects involve complex physical mechanisms, making the achievement of high-performance nonlinear OFCs in a single device a critical unresolved issue.

Here, we introduce a new type of OFC, by collaborating Raman, EO, and Kerr effects in a single LN racetrack microresonator to produce a broadband and flat Raman-electro-optic (REO) microcomb. This novel mechanism, diverging from systems dependent on single nonlinearities, employs Raman scattering and EO modulation to generate diverse EO comb sets, alongside Kerr

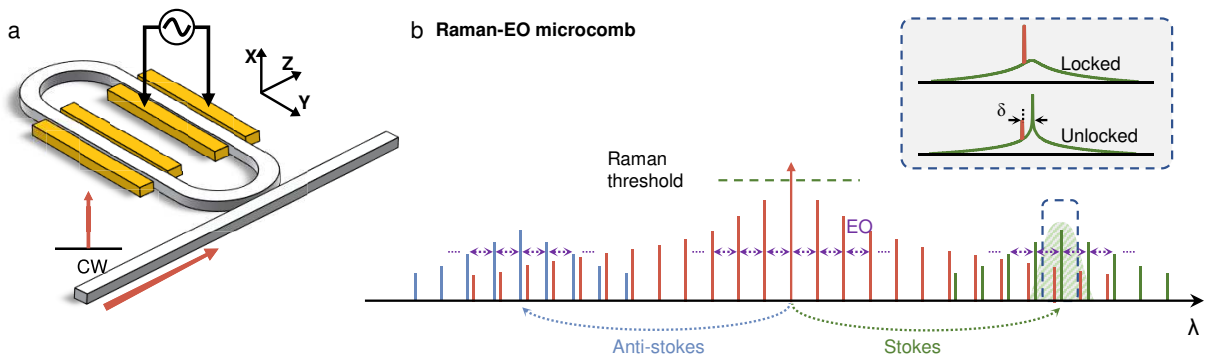


FIG. 1. **Schematic of the hybrid electro-optic comb.** **a.** The EO comb is generated by coupling a continuous-wave (cw) pump laser into a LN resonator under microwave modulation. **b.** Spectrum of the EO comb when the pump laser is below the threshold of Raman lasing. **c.** Spectrum of the EO comb when the pump laser is above the Raman lasing threshold. The EO combs spread around the pump laser and Raman laser share the same  $f_{\text{rep}}$  but have different  $f_{\text{ceo}}$  (unlocked state). With the help of four wave mixing (FWM), these two combs expand their bandwidths and overlap. The beating frequency of the two combs in the overlapped modes is transferred to the Raman laser mode and finally locks the Raman lasing frequency being integer multiples of the microwave frequency from the pump frequency (locked state).

effect augmentation to broaden the spectral range. In particular, comb lines originated from the Raman laser, are self-adaptively phase-locked to the optical and microwave fields without any external electronic feedback loop, ensuring high coherence and fast tunability of the whole microcomb. The resulting broadband REO microcomb, not only showcases an impressive spectral width of 300 nm, but also maintaining a precise repetition rate of 26.03 GHz across nearly 1400 comb lines. Moreover, this microcomb features tunable repetition rates and pump laser frequencies, offering precise control of comb characteristics to enhance performance and broaden application scopes.

## II. SCHEMATIC OF SELF-LOCKED RAMAN-ELECTRO-OPTIC MICROCOMB

Figure 1 illustrates the configuration of the REO microcomb generation based on a LN racktrack microresonator. Efficient coherent energy transfer between adjacent cavity modes occurs when the microwave modulation frequency aligns with the free spectral range (FSR) of the microresonator. This transfer, induced by the electro-optic effect, sequentially shifts the energy of the pump laser to nearby modes one by one, forming the pure EO comb. While increasing the laser pump power enhances the power of all comb lines, it does not affect the EO coupling strength. However, significant Kerr nonlinear processes can arise and help to expand the spectral width by delivering photons to different modes via four-wave mixing (FWM). Meanwhile, as the pump power increases above the Raman threshold, Raman laser can be generated from solely vacuum noise, which further initiates additional EO combs under microwave modulation, as shown in Fig. 1b. However, the frequency of the

Raman lasers depends on the mode detuning and dissipation, thus the frequency difference with the pump laser may not be equal to an integer multiple of the microwave frequency. This leads to a difference ( $\delta$ ) in the carrier-envelope offset frequency  $f_{\text{ceo}}$  between the primary comb and the Raman comb, as shown in the right inset of Fig. 1b. Moreover, the field intensity in the pump mode is clamped due to the threshold nature of the Raman process, which limits the field intensity in all comb lines and eventually the total power and bandwidth of the EO comb.

Fortunately, the collaboration of these nonlinearities provides a route to self-adaptively eliminate the  $\delta$  and merge these combs into a single broader microcomb. The mechanism is organized as follows: (1) Anomalous dispersion in the microresonator enhances FWM, creating overlapping spectral lines between the primary and Raman combs. In the overlap region, there are multiple comb lines in a single mode, with frequencies differed by  $\delta$ ; (2) The Kerr effect transfers this frequency difference  $\delta$  to the Raman gain region, producing a sideband around the Raman laser. The frequency of this sideband differs to the pump laser by integer multiples of the microwave frequency; (3) This sideband competes in the Raman scattering process, potentially serving as a seed for frequency locking. Proper tuning of microwave frequency and pump power can reduce  $\delta$ , leading to the frequency synchronization of the Raman comb lines with the primary comb and the alignment of the  $f_{\text{ceo}}$ , as shown in the inset of Fig. 1b. This process is analogous to laser injection locking [18] but occurs through coherent nonlinear interactions within a single device. As a result of the collaboration of these nonlinearities, the noise from the Raman process is eliminated and the spectral width of the REO microcomb is substantial broadened.

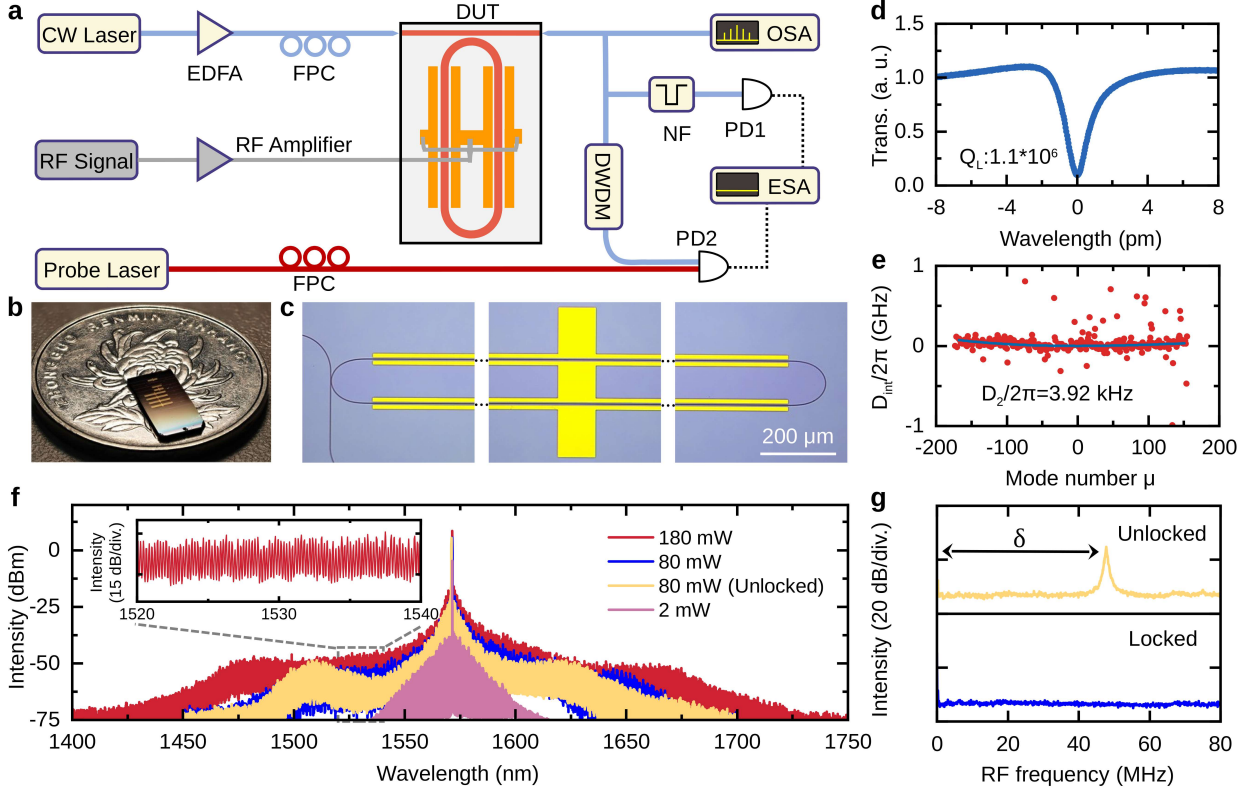


FIG. 2. **a**. Schematic of the experimental setup. EDFA: erdium doped fiber amplifier; FPC: fiber polarization controller; OSA: optical spectrum analyzer; DWDM: dense wavelength division multiplexing; NF: notch filter; ESA: electrical spectrum analyzer. **b**. Photograph of the thin film lithium niobate (TFLN) photonic chip. **c**. The microscope image of the device consisting of a LN racetrack microresonator and electrodes. **d**. The transmission spectrum of a typical fundamental TE mode with a fitted loaded Q-factors of  $1.1 \times 10^6$ . **e**. Red dots are the dispersion of the microresonator around  $1571 \text{ nm}$  measured by the Mach-Zehnder interferometer (MZI). Blue curve is the fitted curve, with the fitted value of  $D_2/2\pi = 3.92 \text{ kHz}$ . **f**. The optical spectra of the hybrid microcomb under different on-chip optical pump power. The driven RF power is 30 dBm. The inset on the upper left corner shows a flat spectrum between  $1520 \text{ nm}$  and  $1540 \text{ nm}$ . **g**. The RF spectra of the output comb field. The disappear of the beating frequency indicates the whole output field being in a phase-locked state.

### III. EXPERIMENTAL SETUP AND MICROCOMB CHARACTERIZATION

The experimental setup is shown in Fig. 2a. The broadband REO microcomb is experimentally demonstrated using an x-cut thin film lithium niobate (TFLN) photonic chip, as shown in Fig. 2b. Figure 2c presents the microscope image of the racetrack microresonator with the FSR of about 26.03 GHz. Detailed information about the device fabrication can be found in the Methods section. The pump laser (Toptica CTL 1550) is amplified and polarization-controlled to match the quasi-TE mode of the on-chip waveguide, and then coupled into the waveguide supporting the fundamental TE mode through a lensed fiber. The transmitted light is collected by another lensed fiber and sent into subsequent characterization instruments. The coupling loss is approximately 6 dB per facet. An RF signal, which matches the FSR of the microresonator, is amplified and applied to

drive the on-chip electrode. Figure 2d shows the pumped mode resonates around the wavelength of  $1571.04 \text{ nm}$  with a loaded Q-factor of  $1.1 \times 10^6$ . The dispersion of the microresonator around  $1571 \text{ nm}$ , shown in Fig. 2e, is analyzed using the integrated dispersion formula  $D_{int} = \frac{1}{2}D_2\mu^2 + \frac{1}{6}D_3\mu^3 + \dots$ , yielding  $D_2/2\pi = 3.92 \text{ kHz}$  indicating anomalous and flat dispersion, which is crucial for expanding the spectral width and locking the microcomb.

Figure 2f displays the optical spectra of microcombs under different pump conditions. At a low on-chip optical pump power of 2 mW, the EO effect predominates, producing a typical EO comb profile with the spectral width of 80 nm with the modulation frequency around 26.03 GHz. When the pump power is increased above the Raman laser threshold, two additional sets of EO combs, corresponding to the Stokes and anti-Stokes EO combs, appear on both sides of the primary comb as shown by the yellow curve in Fig. 2e. With the help

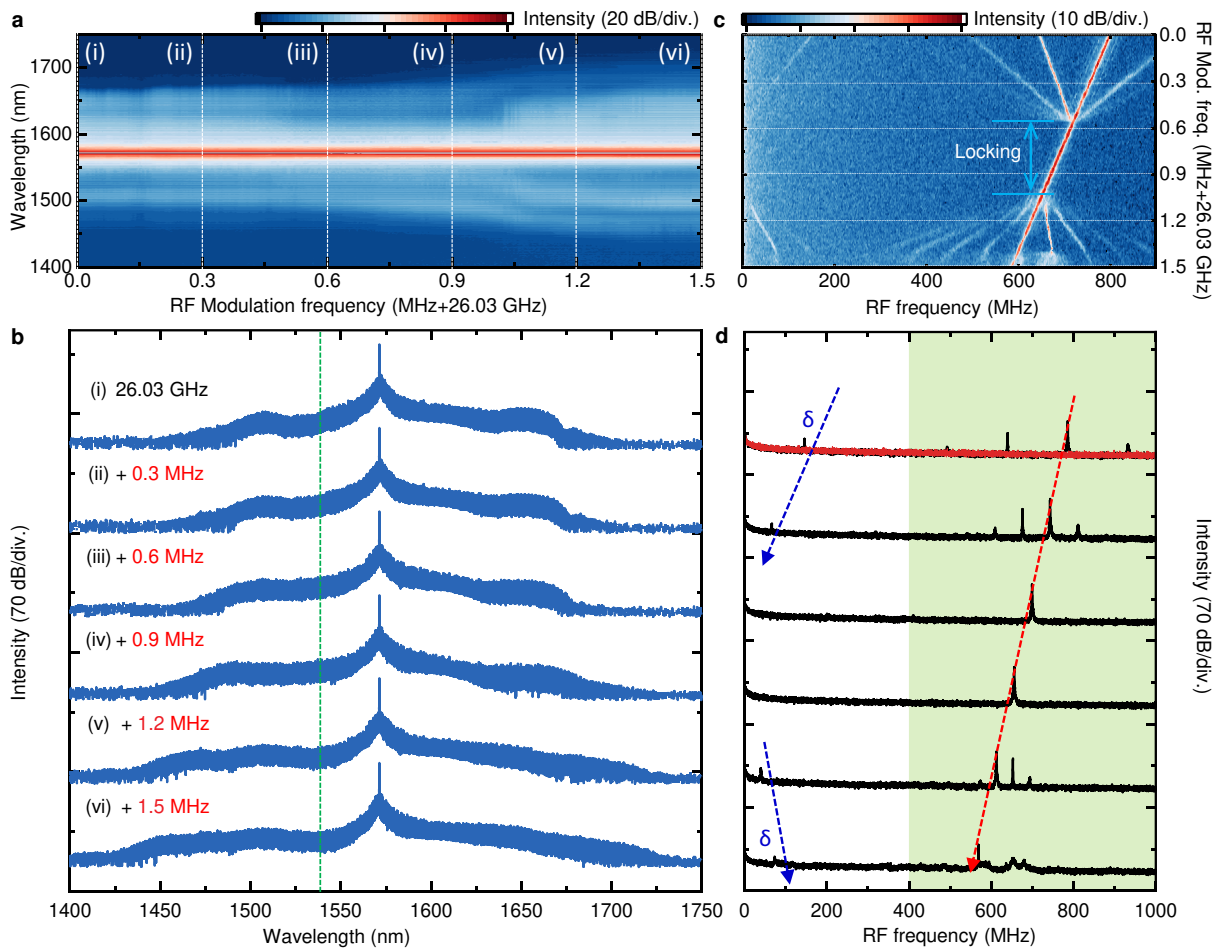


FIG. 3. **a,b.** The evolution of the optical spectra when scanning the microwave modulation frequencies. The green line shows the position of the probe laser. **c,d.** Measured beat note signals between comb lines near the green line and a probe laser at 1541 nm for different microwave frequencies. The corresponding beat note signals captured by an ESA, showcasing three distinct type of spectra, representing self-locked and unlocked states of the hybrid microcomb.

of Raman scattering and FWM, the spectral width of the hybrid comb becomes significantly wider compared to the pure EO comb at low pump power. After filtering out the pump laser, the output comb field is injected to the photodetector (PD) and analyzed by the electrical spectrum analyzer (ESA). A beat signal in the upper panel of the Fig. 2g, indicates a frequency difference  $\delta$  of about 48 MHz between the primary comb line and the Raman comb line within the same resonance mode, implying distinct frequency offsets  $f_{\text{ceo}}$  and preventing treatment as a single phase-locked comb. This beating frequency depends on the pump and microwave driving conditions as well as environment noise. Through adjusting the microwave modulation frequency to reduce the  $\delta$ , an abrupt disappearance of the beat signal reveals that these combs is merged into a single one (lower panel of the Fig. 2g). The locked REO microcomb shows a broad spectral width and obvious flatness along the wings, as well as an overall higher field intensity of all comb lines (blue curve in Fig. 2f). With further increasing optical

pump power to 180 mW, more significant Kerr effect can expand the spectral width further to over 300 nm.

#### IV. LOCKING BEHAVIOR OF THE MICROCOMB

To characterize the self-locked state of the REO microcomb and exclude any accidental alignment of the primary and Raman combs, we experimentally investigate the locking dynamics by varying the microwave frequency under fixed optical pump power (150 mW) and modulation power (30 dBm). The microwave modulation frequency starts at 26.03 GHz. As the modulation frequency is increased to better match the FSRs near the pumped mode, the spectral width of the entire microcomb broadens progressively, as illustrated in Fig. 3a. Meanwhile, the intensity peak of the comb lines gradually shifts from longer to shorter wavelengths (from Stokes to anti-Stokes comb). This shift is attributed to the anomalous dis-



persion of the microresonator, where the FSR increases from longer to shorter wavelengths. Figure 3b provides a detailed view of how the spectral intensity distribution varies with the modulation frequency.

Limited by the resolution of the OSA, the details around the overlap region are challenging to discern. Therefore, a probe laser around 1541 nm is employed to detect the comb lines in the overlap region. The probed comb lines near 1541 nm are extracted by filtering other comb lines using dense wavelength division multiplexing (DWDM). The corresponding beat signals are displayed in Fig. 3c, d. There are two distinct groups of beat signals in the RF spectra. The lower one, corresponding to the frequency difference  $\delta$  between comb lines, gradually decreases and disappears with increasing the modulation frequency, and then reappears after hundreds of kHz, as indicated by the blue dashed line in Fig. 3d. The disappeared region corresponds to the locking range, which can also be confirmed by the beat signal of the probe laser with the comb lines in the nearest cavity mode, i.e., another group of beat signals at higher frequency. The central peak of this group of beat signals, marked in red dashed line in Fig. 3d, represents the comb line from the primary comb, and the slope of this red dashed line represents the mode index of the probed mode relative to the pumped mode. The peak spacing equals to the offset difference  $\delta$ , which scales linearly with the microwave frequency. When the modulation frequency is outside the locking range, both the primary and Raman comb lines coexist within the cavity mode, along with their FWM generated sidebands. Otherwise, there is only one single comb line within the cavity mode. The sudden shift of the beat signals and its dependence on the microwave frequency are clear indicators of the self-locking process. The width of the corresponding locking range can reach 520 kHz, indicating the robustness of the self-locked microcomb against small variations in the pump and microwave fields as well as environment fluctuations. The self-locked microcomb exhibits a flat distribution of comb lines at its wings, which is attributed to the effect of Raman gain and Kerr effect. Furthermore, the self-locking mechanism also reduces Raman noise (see Supplementary Information), as widely seen in injection locking experiments [18]. In this way, the self-locking mechanism transforms the typically harmful Raman scattering into a beneficial nonlinear gain mechanism for broadband EO comb generation.

Indeed, the locking range of the microcomb offers a precise tuning method for fine-tuning  $f_{\text{rep}}$  across several hundred kHz. To realize extensive tuning of  $f_{\text{rep}}$ , it is necessary to demonstrate that the microcomb can remain locked under various microwave frequencies that are significantly different. By adjusting the pump laser frequency, the locking range can be changed, as depicted in Fig. 4a. It is observed that the locking range gradually shifts to lower frequency as the pump laser frequency

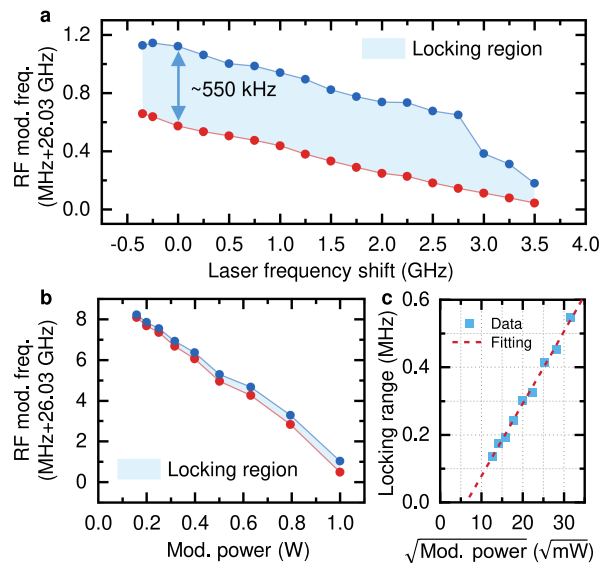


FIG. 4. **a.** Measured beat note signal by a probe laser at 1541 nm for different pump laser frequencies. The comb is self-locked in the shaded region between the two lines. The locking range shift with laser frequency shift, demonstrating the self-locked comb works for various  $f_{\text{rep}}$ . **b.** Relationship between the locking range and the modulation power. **c.** Relationship between the microwave amplitude and the locking range, which is well fitted by a linear function.

is decreased, due to the diminishing frequency difference between the pump laser and the Raman laser. When the pump laser frequency is excessively high, the detuning between the pump laser and the cavity mode becomes too large, resulting in insufficient intracavity power to transfer the offset difference  $\delta$  to the Raman laser mode, thus reducing the locking region. Conversely, when the pump laser frequency is too low, the pump laser shifts to the red-detuned side of the cavity mode, causing it to exit the cavity mode. The upper and lower boundaries at different laser frequencies define a locking region, within which the locking range exceeds 500 kHz for most laser frequencies, with the largest range reaching 550 kHz.

In addition to the optical tuning method, the microwave energy can heat the chip, thus changing the FSR of the microresonator via the thermal effect. This alteration significantly impacts the locking behavior of the microcomb. Figure 4b illustrates how the two boundaries of the locking range shift when the microwave modulation power is adjusted from 21 dBm to 30 dBm, showing that the locking frequency can vary within a range of 8 MHz. From the data in Fig. 4b, we also analyzed the relationship between the width of the locking range and the modulation power. Since the comb line amplitude is proportional to microwave amplitude of the EO modulation, a larger microwave amplitude leads to an extended locking range. As depicted in the Fig. 4c, the locking range exhibits a positive relationship with the microwave

amplitude, fitting well to a linear function.

## V. CONCLUSION

In conclusion, we have demonstrated the generation of a broadband REO microcomb in a single LN microresonator, achieving a spectral width exceeding 300 nm and more than 1400 comb lines at a 26.03 GHz repetition rate. By utilizing the cooperation between Kerr, Raman and EO nonlinearities, we have addressed the spectral width and noise limitation imposed by Raman scattering, transforming it into a beneficial nonlinear process that enhances the width and the flatness of the optical spectrum. The resulting microcomb is not only broadband but also highly tunable and capable of rapid on-chip modulation with a  $f_{\text{rep}}$  tuning ranging of 8 MHz. These characteristics make it an indispensable tool in applications ranging from high-resolution spectroscopy to advanced telecommunications and quantum information processing. To further expand the spectral width and tunability of this microcomb, enhancing the self-locking capability by increasing the pump conversion efficiency [32], engineering dispersive waves at the overlap region, and utilizing higher-order Raman processes are recommended. The self-locking mechanism can also be adapted for other parametric and competitive nonlinear processes, such as  $\chi^{(2)}$  and  $\chi^{(3)}$  parametric oscillation, Brillouin scattering and lasing process. Given the ubiquity of different nonlinearities in integrated nonlinear photonics, our findings may inspire further research into exploiting these interactions to develop novel nonlinear photonic devices.

## Methods

### Device fabrication

The device is fabricated on a commercial x-cut thin film lithium niobate (TFLN) wafer (NANOLN). The 600-nm-thick TFLN is bonded to a silicon substrate with 500- $\mu\text{m}$ -thick silicon and 2- $\mu\text{m}$ -thick wet oxidation silicon dioxide ( $\text{SiO}_2$ ). Electron-beam lithography is used to define the pattern of the device with hydrogen-silsesquioxane (HSQ) resist. Then, the film is partially etched by argon-ion-based reactive ion etching in an inductively coupled plasma (ICP) etcher to form a 350-nm-depth trapezoidal waveguide cross section with a remaining slab of 250 nm. The whole chip is cleaned by buffered HF solution and RCA1 cleaning solution ( $\text{NH}_3:\text{H}_2\text{O}_2:\text{H}_2\text{O} = 1:1:5$ ) to remove the remaining HSQ resist and the redeposition formed in the etching process. The gold modulation electrodes are patterned using laser direct writing and the metal (15 nm of chromium, 300 nm of gold) is transferred using thermal evaporation and the bilayer lift-off process. The LN racetrack microresonator used in experiments has a top width of 1.4  $\mu\text{m}$  and a side-wall angle of around 60°. The fiber-to-chip coupling loss is approximately 6 dB per facet.

## Data availability

All data generated or analyzed during this study are available within the paper. Further source data will be made available on request.

---

\* These authors contributed equally to this work.

† [bofang@nankai.edu.cn](mailto:bofang@nankai.edu.cn)

‡ [chunhua@ustc.edu.cn](mailto:chunhua@ustc.edu.cn)

- [1] T. J. Kippenberg, R. Holzwarth, and S. A. Diddams, “Microresonator-based optical frequency combs,” *Science* **332**, 555 (2011).
- [2] S. A. Diddams, K. Vahala, and T. Udem, “Optical frequency combs: Coherently uniting the electromagnetic spectrum,” *Science* **369**, 267 (2020).
- [3] J. Liu, F. Bo, L. Chang, C.-H. Dong, X. Ou, B. Regan, X. Shen, Q. Song, B. Yao, W. Zhang, *et al.*, “Emerging material platforms for integrated microcavity photonics,” *Science China Physics, Mechanics & Astronomy* **65**, 104201 (2022).
- [4] T. J. Kippenberg, A. L. Gaeta, M. Lipson, and M. L. Gorodetsky, “Dissipative kerr solitons in optical microresonators,” *Science* **361** (2018).
- [5] A. L. Gaeta, M. Lipson, and T. J. Kippenberg, “Photonic-chip-based frequency combs,” *Nature Photonics* **13**, 158 (2019).
- [6] L. Chang, S. Liu, and J. E. Bowers, “Integrated optical frequency comb technologies,” *Nature Photonics* **16**, 95 (2022).
- [7] D. T. Spencer, T. Drake, T. C. Briles, J. Stone, L. C. Sinclair, C. Fredrick, Q. Li, D. Westly, B. R. Ilic, A. Bluestone, *et al.*, “An optical-frequency synthesizer using integrated photonics,” *Nature* **557**, 81 (2018).
- [8] J. Liu, E. Lucas, A. S. Raja, J. He, J. Riemensberger, R. N. Wang, M. Karpov, H. Guo, R. Bouchand, and T. J. Kippenberg, “Photonic microwave generation in the x- and k-band using integrated soliton microcombs,” *Nature Photonics* **14**, 486 (2020).
- [9] P. Marin-Palomo, J. N. Kemal, M. Karpov, A. Kordts, J. Pfeifle, M. H. Pfeiffer, P. Trocha, S. Wolf, V. Brasch, M. H. Anderson, *et al.*, “Microresonator-based solitons for massively parallel coherent optical communications,” *Nature* **546**, 274 (2017).
- [10] B. Corcoran, M. Tan, X. Xu, A. Boes, J. Wu, T. G. Nguyen, S. T. Chu, B. E. Little, R. Morandotti, A. Mitchell, *et al.*, “Ultra-dense optical data transmission over standard fibre with a single chip source,” *Nature Communications* **11**, 1 (2020).
- [11] B. Wang, J. S. Morgan, K. Sun, M. Jahanbozorgi, Z. Yang, M. Woodson, S. Estrella, A. Beling, and X. Yi, “Towards high-power, high-coherence, integrated photonic mmwave platform with microcavity solitons,” *Light: Science & Applications* **10**, 4 (2021).
- [12] R. Niu, M. Li, S. Wan, Y. R. Sun, S.-M. Hu, C.-L. Zou, G.-C. Guo, and C.-H. Dong, “khz-precision wavemeter based on reconfigurable microsoliton,” *Nature Communications* **14**, 1 (2023).
- [13] X. Xu, M. Tan, B. Corcoran, J. Wu, A. Boes, T. G. Nguyen, S. T. Chu, B. E. Little, D. G. Hicks, R. Morandotti, A. Mitchell, and D. J. Moss, “11 TOPS photonic

- convolutional accelerator for optical neural networks,” *Nature (London)* **589**, 44 (2021).
- [14] J. Feldmann, N. Youngblood, M. Karpov, H. Gehring, X. Li, M. Stappers, M. Le Gallo, X. Fu, A. Lukashchuk, A. S. Raja, J. Liu, C. D. Wright, A. Sebastian, T. J. Kippenberg, W. H. P. Pernice, and H. Bhaskaran, “Parallel convolutional processing using an integrated photonic tensor core,” *Nature (London)* **589**, 52 (2021).
- [15] S. A. Diddams, D. J. Jones, J. Ye, S. T. Cundiff, J. L. Hall, J. K. Ranka, R. S. Windeler, R. Holzwarth, T. Udem, and T. W. Hänsch, “Direct link between microwave and optical frequencies with a 300 thz femtosecond laser comb,” *Physics Review Letters* **84**, 5102 (2000).
- [16] D. J. Jones, S. A. Diddams, J. K. Ranka, A. Stentz, R. S. Windeler, J. L. Hall, and S. T. Cundiff, “Carrier-envelope phase control of femtosecond mode-locked lasers and direct optical frequency synthesis,” *Science* **288**, 635 (2000).
- [17] T. Udem, R. Holzwarth, and T. W. Hänsch, “Optical frequency metrology,” *Nature* **416**, 233 (2002).
- [18] B. Shen, L. Chang, J. Liu, H. Wang, Q.-F. Yang, C. Xiang, R. N. Wang, J. He, T. Liu, W. Xie, J. Guo, D. Kinghorn, L. Wu, Q.-X. Ji, T. J. Kippenberg, K. Vahala, and J. E. Bowers, “Integrated turnkey soliton microcombs,” *Nature* **582**, 365 (2020).
- [19] M. Rowley, P.-H. Hanzard, A. Cutrona, H. Bao, S. T. Chu, B. E. Little, R. Morandotti, D. J. Moss, G.-L. Oppo, J. S. Toterogongora, M. Peccianti, and A. Pasquazi, “Self-emergence of robust solitons in a microcavity,” *Nature (London)* **608**, 303 (2022).
- [20] T. C. Briles, S.-P. Yu, L. Chang, C. Xiang, J. Guo, D. Kinghorn, G. Moille, K. Srinivasan, J. E. Bowers, and S. B. Papp, “Hybrid inp and sin integration of an octave-spanning frequency comb,” *APL Photonics* **6**, 026102 (2021).
- [21] C. Xiang, J. Liu, J. Guo, L. Chang, R. N. Wang, W. Weng, J. Peters, W. Xie, Z. Zhang, J. Riemensberger, J. Selvidge, T. J. Kippenberg, and J. E. Bowers, “Laser soliton microcombs heterogeneously integrated on silicon,” *Science* **373**, 99 (2021).
- [22] M. Zhang, B. Buscaino, C. Wang, A. Shams-Ansari, C. Reimer, R. Zhu, J. M. Kahn, and M. Lončar, “Broadband electro-optic frequency comb generation in a lithium niobate microring resonator,” *Nature* **568**, 373 (2019).
- [23] D. Zhu, C. Chen, M. Yu, L. Shao, Y. Hu, C. Xin, M. Yeh, S. Ghosh, L. He, C. Reimer, *et al.*, “Spectral control of nonclassical light pulses using an integrated thin-film lithium niobate modulator,” *Light: Science & Applications* **11**, 327 (2022).
- [24] C. Wang, M. Zhang, X. Chen, M. Bertrand, A. Shams-Ansari, S. Chandrasekhar, P. Winzer, and M. Lončar, “Integrated lithium niobate electro-optic modulators operating at CMOS-compatible voltages,” *Nature* **562**, 101 (2018).
- [25] M. He, M. Xu, Y. Ren, J. Jian, Z. Ruan, Y. Xu, S. Gao, S. Sun, X. Wen, L. Zhou, L. Liu, C. Guo, H. Chen, S. Yu, L. Liu, and X. Cai, “High-performance hybrid silicon and lithium niobate Mach-Zehnder modulators for 100 Gbit s<sup>-1</sup> and beyond,” *Nature Photonics* **13**, 359 (2019).
- [26] R. F. Schaufele and M. J. Weber, “Raman Scattering by Lithium Niobate,” *Physical Review* **152**, 705 (1966).
- [27] M. Leidinger, B. Sturman, K. Buse, and I. Breunig, “Strong forward-backward asymmetry of stimulated Raman scattering in lithium-niobate-based whispering gallery resonators,” *Optics Letters* **41**, 2823 (2016).
- [28] Y. He, R. Lopez-Rios, U. A. Javid, J. Ling, M. Li, S. Xue, K. Vahala, and Q. Lin, “High-speed tunable microwave-rate soliton microcomb,” *Nature Communications* **14**, 3467 (2023).
- [29] Z. Gong, X. Liu, Y. Xu, M. Xu, J. B. Surya, J. Lu, A. Bruch, C. Zou, and H. X. Tang, “Soliton microcomb generation at 2  $\mu\text{m}$  in z-cut lithium niobate microring resonators,” *Optics Letters* **44**, 3182 (2019).
- [30] Z. Gong, M. Li, X. Liu, Y. Xu, J. Lu, A. Bruch, J. B. Surya, C. Zou, and H. X. Tang, “Photonic Dissipation Control for Kerr Soliton Generation in Strongly Raman-Active Media,” *Phys. Rev. Lett.* **125**, 183901 (2020).
- [31] C. Wang, Z. Li, J. Riemensberger, G. Lihachev, M. Churraev, W. Kao, X. Ji, T. Blesin, A. Davydova, Y. Chen, X. Wang, K. Huang, X. Ou, and T. J. Kippenberg, “Lithium tantalate photonic integrated circuits for volume manufacturing,” *Nature* **629**, 784 (2024).
- [32] Y. Hu, M. Yu, B. Buscaino, N. Sinclair, D. Zhu, R. Cheng, A. Shams-Ansari, L. Shao, M. Zhang, J. M. Kahn, and M. Lončar, “High-efficiency and broadband on-chip electro-optic frequency comb generators,” *Nature Photonics* **16**, 679 (2022).

### Acknowledgments

The authors thank C.-L. Zou for helpful discussions. The work was supported by the National Natural Science Foundation of China (12293052, 11934012, 12104442, 92050109, 12374361, and 92250302), Innovation program for Quantum Science and Technology (2021ZD0303203), the CAS Project for Young Scientists in Basic Research (YSBR-069), the Fundamental Research Funds for the Central Universities and the USTC Research Funds of the Double First-Class Initiative. This work was partially carried out at the USTC Center for Micro and Nanoscale Research and Fabrication.

### Author contributions

S. W., P.-Y. W. and M. L. contribute equally to this work. C.-H. D. and S. W. conceived the experiments, S. W., P.-Y. W., R. M., and F. B. prepared devices, S. W., P.-Y. W. and R. N. built the experimental setup and carried out measurements, with assistance from F.W.S. M.L. provided theoretical supports. S. W., M. L. and C.-H.D. wrote the manuscript with input from all co-authors. C.-H.D. and G.-C.G. supervised the project. All authors contributed extensively to the work presented in this paper.

### Competing financial interests

The authors declare no competing financial interests.